Bioactive Materials 8 (2022) 95–108

Contents lists available at ScienceDirect

Bioactive Materials

journal homepage: www.sciencedirect.com/journal/bioactive-materials

Magnesium implantation or supplementation ameliorates bone disorder in CFTR-mutant mice through an ATF4-dependent Wnt/β-catenin signaling

Jiankun Xu [a,1], Peijie Hu [b,1], Xiaotian Zhang [b], Junjiang Chen [b,c], Jiali Wang [a,d], Jieting Zhang [c], Ziyi Chen [a,c], Mei Kuen Yu [b,c], Yiu Wa Chung [c], Yan Wang [c], Xiaohu Zhang [c], Yifeng Zhang [a,e], Nianye Zheng [a], Hao Yao [a], Jiang Yue [a], Hsiao Chang Chan [c], Ling Qin [a,*], Ye Chun Ruan [b,**]

[a] Musculoskeletal Research Laboratory, Department of Orthopedics & Traumatology, The Chinese University of Hong Kong, Hong Kong, China
[b] Deparment of Biomedical Engineering, Faculty of Engineering, The Hong Kong Polytechnic University, Hong Kong, China
[c] Epithelial Cell Biology Research Centre, School of Biomedical Sciences, Faculty of Medicine, The Chinese University of Hong Kong, Hong Kong, China
[d] School of Biomedical Engineering, Sun Yat-sen University, Guangzhou, China
[e] School of Life Science and Technology, ShanghaiTech University, Shanghai, China

ARTICLE INFO

Keywords:
Magnesium implant
Cystic fibrosis-related bone disorder
ATF4
Wnt/β-catenin signaling

ABSTRACT

Magnesium metal and its alloys are being developed as effective orthopedic implants; however, the mechanisms underlying the actions of magnesium on bones remain unclear. Cystic fibrosis, the most common genetic disease in Caucasians caused by the mutation of CFTR, has shown bone disorder as a key clinical manifestation, which currently lacks effective therapeutic options. Here we report that implantation of magnesium-containing implant stimulates bone formation and improves bone fracture healing in CFTR-mutant mice. Wnt/β-catenin signaling in the bone is enhanced by the magnesium implant, and inhibition of Wnt/β-catenin by iCRT14 blocks the magnesium implant to improve fracture healing in CFTR-mutant mice. We further demonstrate that magnesium ion enters osteocytes, increases intracellular cAMP level and activates ATF4, a key transcription factor known to regulate Wnt/β-catenin signaling. *In vivo* knockdown of ATF4 abolishes the magnesium implant-activated β-catenin in bones and reverses the improved-fracture healing in CFTR-mutant mice. In addition, oral supplementation of magnesium activates ATF4 and β-catenin as well as enhances bone volume and density in CFTR-mutant mice. Together, these results show that magnesium implantation or supplementation may serve as a potential anabolic therapy for cystic fibrosis-related bone disease. Activation of ATF4-dependent Wnt/β-catenin signaling in osteocytes is identified as a previously undefined mechanism underlying the beneficial effect of magnesium on bone formation.

1. Introduction

Magnesium, an essential nutritional element, is increasingly recognized as beneficial for the health of musculoskeletal system [1–4]. Magnesium metal and its alloys are proven to be biocompatible, biodegradable, and osteo-promotive, and therefore are being developed as effective orthopedic implants to treat bone fractures and osteonecrosis in the clinic [5–8]. We recently reported that orthopedic implant-derived magnesium improves bone fracture healing in rats by promoting neuronal production of CGRP (calcitonin gene-related peptide) [1,9]. However, other potential actions of magnesium on bones, directly or indirectly, remain largely unexplored.

Cystic fibrosis (CF), resulting from mutations in the gene encoding the anion-channel CFTR (cystic fibrosis transmembrane conductance regulator), is the most common lethal genetic disease in Caucasians [10,11]. Although CF is primarily regarded as a lung disease with a defect in airway epithelial function, a broad range of organs are affected in the disease progression [12–14]. For example, osteopenia or osteoporosis with bone fracture is commonly reported in individuals with CF, the so-called CF-related bone disease (CFBD) [15–17]. Though CFBD is not

Peer review under responsibility of KeAi Communications Co., Ltd.
* Corresponding author.
** Corresponding author.
E-mail addresses: lingqin@cuhk.edu.hk (L. Qin), sharon.yc.ruan@polyu.edu.hk (Y.C. Ruan).
[1] These authors contributed equally.

https://doi.org/10.1016/j.bioactmat.2021.06.034
Received 11 April 2021; Received in revised form 26 June 2021; Accepted 27 June 2021
Available online 3 July 2021
2452-199X/© 2021 The Authors. Publishing services by Elsevier B.V. on behalf of KeAi Communications Co. Ltd. This is an open access article under the CC BY-NC-ND license (http://creativecommons.org/licenses/by-nc-nd/4.0/).

directly lethal for such patients, the condition is believed to exacerbate respiratory dysfunction due to rib and vertebral problems, as well as to worsen nutritional status, contributing to the mortality of CF [16,18]. Despite recent improvements in the pharmacological treatment of CF [19], the disease remains incurable. Bone fragility also precludes possible lung-transplantation, often a life-saving operation, in severe cases of CF [16]. As parathyroid hormone and 25-hydroxyvitamin D levels are reported to be normal in CFBD [20] and current strategies for CFBD (e.g. vitamin D and calcium supplementation, anti-resorptive agents) are of limited or controversial effects [21], an efficient treatment for CFBD is an important unmet clinical need.

Interestingly, magnesium deficiency or metabolism disturbance has been documented in individuals with CF of advanced age or of severe pathology [22]. Intracellular Mg^{2+} is also critically involved in CFTR channel function [23]. In the present study, we tested the potential of magnesium (both implant-derived and oral supplementation) in rescuing bone pathology in CFTR deficient mice. Our results show that magnesium, through activating ATF4 and promoting CFTR deficiency-impaired Wnt/β-catenin signaling, elevated bone volume, bone mineral density (BMD), and biomechanical strength as well as fracture healing, revealing a previously undefined role of magnesium in bones.

2. Materials and methods

2.1. Animals

C57BL/6 and ΔF508 mice harboring the mutation of CFTR were obtained from the Laboratory Animal Service Centre of the Chinese University of Hong Kong and maintained with a 12-h light-dark cycle and constant temperature (25 °C). All animal experiments were conducted in accordance with ethical approvals at Hong Kong Polytechnic University (17–18/15-BME-R-HMRF) and the Chinese University of Hong Kong (15-207-MIS-5C). When necessary, intraperitoneal injection of ketamine (75 mg/kg body weight) and xylazine (10 mg/kg body weight) was used to anesthetize mice.

2.2. Cell culture

MC3T3-E1 subclone 4 (ATCC, CRL-2593) and MLO-Y4 (Karafast, EKC002) were cultured in Alpha Minimum Essential Medium (Gibco, 11900024) supplied with fetal bovine serum (5% for MLO-Y4 and 10% for MC3T3-E1, Gibco, 10270106), penicillin (100 U/mL) and streptomycin (100 μg/mL, Gibco, 15140122) at 37 °C in 5% CO_2 incubator.

2.3. RNA extraction & quantitative PCR

Femoral bones were harvested from mice. After soft tissues were carefully removed, the proximal femoral tissues were minced in liquid nitrogen into powder before collected into TRIzol (Invitrogen, 15596018) for RNA extraction according to the manufacturer's instructions. Nanodrop spectrophotometer (Thermo, ND-ONE-W) was used to determine the RNA quantity and purity. 1 μg of total RNA was reverse-transcribed into cDNA using a high-capacity cDNA Reverse Transcription Kit (Thermo, 4368814), which was then amplified by SYBR Green Premix Ex Taq™ Mix (Takara, RR420A) and primers (listed in Supplementary Table), and analyzed using the Bio-Rad real-time PCR system (Bio-Rad, CFX96). mRNA expression of the target genes was normalized with that of *Gapdh*, and analyzed using the $2^{-\Delta\Delta Cq}$ method.

2.4. Quantitative PCR array

5 μg of total RNA was reverse-transcribed into cDNA and used for each plate of Wnt Signaling Targets RT^2 Profiler PCR Array (Qiagen, PAMM-243ZA). Amplification was done by using Bio-Rad real-time PCR system (CFX96) or ABI QuantStudio 12K Flex Real-Time PCR System (Applied Biosystems) following the manufacturers' instructions. The expressions of target genes were normalized with the average expression of the house-keeping genes in the array plate. Relative gene expression fold was calculated using the $2^{-\Delta\Delta Cq}$ formula.

2.5. Dual-energy X-Ray absorptiometry (DXA) analysis

After anesthetization with intraperitoneal injection of ketamine (75 mg/kg body weight) and xylazine (10 mg/kg body weight), mice were whole-body scanned by the UltraFocusDXA Digital Radiography System (Faxitron, USA) at high-resolution with x-rays at two energy levels (40 and 70 kVp). The bone mineral density (BMD) and bone mineral content (BMC) of the selected region of interest (ROI) were calculated by Faxitron Bioptics Vision software (version 2.3.2).

2.6. Intramedullary implantation model

Age-matched male wild-type and ΔF508 mice were used. As we previously described [9], after anesthetization of the mice, the right knee was surgically exposed before a tunnel of 0.6-mm in diameter was drilled starting from the patellofemoral groove of the distal femur along the axis of the femoral shaft. A sterilized magnesium or stainless steel rod was then inserted through the drilled tunnel into the femur canal. Wounds were closed by sutures afterwards. Radiographs of the operated distal femora were taken to monitor the bone formation.

2.7. Fabrication of the magnesium-inserted intramedullary nail (Mg-IMN)

We purchased 23 G spinal needles (hollow, outer diameter: 0.6 mm; inner diameter: 0.4 mm) from the Terumo company (Terumo, USA). The needles were further sent to Ziyoujian (Shenzhen, China) for drilling holes using electrical sparks burning along vertical directions at the transverse section, with an equal distance of 0.25 mm between each hole. Afterwards, we inserted an ultrapure magnesium rod with a diameter of 0.4 mm into the hollow needles to resemble the Mg-IMN. The holes on the wall of the needles served as windows for the release of magnesium ions.

2.8. Closed-fracture model in mice

Age-matched female wild-type and ΔF508 mice were randomly assigned to Mg-IMN and IMN groups, respectively. Under general anesthesia, following drilling and reaming with a 23 G needle (0.6 mm in diameter), a Kirschner wire (0.5 mm in diameter, K wire) was inserted into the medullary canal retrogradely. To make a fracture on the mid-shaft of the femur, we used a custom-made 3-point-bending apparatus, with a metallic blade (weighted about 50 g) dropping from a height of 25 cm. After confirming that the fracture gap was smaller than 0.5 mm and displacement <0.5 mm using anteroposterior (A-P) and lateral radiographies, we replaced the K-wire with a 23 G needle (containing Mg rod or not) and perforated the proximal femur through the piriformis fossa and blended the tip of the needle to leave a 3 mm length to prevent implant movement. We also cut the distal end of the needle at the level of the articular surface to allow free joint movement. We sutured the wound by layers and gave analgesia (temgesic) every day for 3 days post fracture to reduce the pain suffering in animals.

2.9. Micro-CT analysis

Femora or lumbar vertebra were harvested. The stainless steel was removed according to our well-established protocol [9]. Briefly, the bone specimens were collected after the mice were sacrificed. Since the stainless-steel implant has a smooth surface and little osteointegration, it would not be erupted inside the medullary cavity during the implantation period and were removed using a tweezer or forceps. The removal

of the stainless-steel implant or IMN (intramedullary nail) did not affect the bone quality. Samples were wrapped in wet gauze and fitted in the sample tube to process for micro-CT scanning (μCT40, Scanco Medical, Brüttisellen, Switzerland). The scan range was set to be 10 mm (for the mid-shaft of intact femora from mice), 15 mm (for both fractured femora from mice with the fracture line defined as the mid-plane within this range, and for the mid-shaft of intact femora from rats), 5 mm (for lumbar vertebra from both mice and rats). We set the resolution at 15 μm per voxel and 1024 × 1024 pixels. We selected the region of interest (ROI) from 2D images with thresholds set at >220 for intact femora, >180 for fractured femora as mineralized tissue, according to the tuning. We also conducted 3D reconstruction of the mineralized tissue with a low-pass Gaussian filter (Sigma = 0.8, Support = 1.0), according to our established protocol [9]. We conducted quantitative analysis by integrating all 2D images. For cortical bone, morphometric parameters included total BV, TV, BV/TV and BMD of BV. In addition to these parameters, for trabecular bone, Trab.N and Trab.Th were also analyzed.

2.10. Histomorphometric analysis

We evaluated bone formation rate using sequential calcein/xylenol fluorescence double labeling [9]. Firstly, we conducted intraperitoneal injection of Calcein green (5 mg/kg body weight, Sigma-Aldrich, USA) for the mice at 7 days before the injection of xylenol orange (90 mg/kg body weight, Sigma-Aldrich, USA). Another 3 days afterwards, we sacrificed the mice to harvest their femora. The undecalcified samples were further embedded in MMA and sectioned (about 200 μm thick), according to our established protocol [24]. The thick sections were further polished to 100 μm for evaluating new-bone formation rate (BFR/BS) and mineral apposition rate (MAR) under a fluorescent microscope (DM5500 B, Leica) integrated with the OsteoMeasure™ Histomorphometry Systems (Osteometrics Inc) as previously described [9].

2.11. Radiographic analysis of fracture callus

Complete bridging of the mineralized callus was recognized as radiographic healing. Callus area was defined as the radiopaque area as measured on a lateral radiograph of each mouse by using ImageJ (NIH). Triple measurements were performed for each callus and the average was used for statistical analysis.

2.12. Detection of bone turnover markers, osteocalcin and ALP activity by ELISA

Serum samples were collected for the quantitative detection of procollagen I N-terminal peptide (PINP) (abbexa, UK) and C-terminal telopeptides of type I collagen (CTX) (abbexa, UK), osteocalcin (Abcam, USA), and ALP (Abcam, USA) ELISA kits according to the instructions. Finally, we normalized the ELISA result using the concentration of total protein for each specimen.

2.13. Histological analysis

Femora from mice were collected, fixed by 4% paraformaldehyde (PFA) for 2 days, decalcified in 9% formic acid for 2 weeks with the aid of ultrasound, according to our established protocol [24]. After dehydrated in a series of ethanol and xylene, the samples were embedded with paraffin. Sections (5 μm in thickness) were prepared and processed to H&E for the evaluation of healing under light microscope (DM5500 B, Leica). Polished non-decalcified sections (100 μm in thickness) were also evaluated by *von kossa* staining.

2.14. Biomechanical test

We adopted three-point bending biomechanical test to investigate the fracture-healing quality using a testing machine installed in our laboratory (H25KS Hounsfield Test Equipment, Redhill, Surrey, UK). In brief, we placed the femora with the anterior–posterior direction on the lower supporting bars with a distance of 12.5 mm, flanking the fracture callus. Then we applied a load (250 N cell) at a compression speed of 5 mm/min until failure. We recorded the maximum compressive load according to the load-deformation curve in the built-in QMAT software (Redhill, Surrey, UK).

2.15. Immunohistochemistry analysis

Femora from mice were harvested, fixed by 4% paraformaldehyde (PFA) for two days, and decalcified in 9% formic acid for 2 weeks. After dehydrated in a series of ethanol and xylene, they were embedded in paraffin and cut into sections with a thickness of 5 μm for processing to immunohistochemical staining. Antibodies against non-phospho (Active) β-catenin (1:1000, Cell Signaling, 8814), ATF4/CREB-2 (1:200, Santa Cruz, sc390063), and CGRP (1:200, Abcam, ab47027) were used to incubate separate sections overnight, in cold room (4 °C). HRP-conjugated secondary antibodies against the species of primary antibodies under a dilution of 1:400 (v/v) were incubated for 1 h at room temperature. Then the HRP signals were visualized using DAB Substrate Kit (Abcam, ab64238). For immunostaining in cultured cells, cells were firstly fixed with 4% PFA for 20–30 min before treated with Triton X (0.01%) and SDS (1%) in PBS for 20 min, blocked and incubated with antibodies (following the protocols described above).

2.16. Western blotting

We lysed the cells or tissues in ice-cold RIPA lysis buffer (150 mM NaCl, 50 mM Tris-Cl, 1% NP-40, 0.5% DOC and 0.1% SDS, pH 7.5) supplemented with cocktails containing protease and phosphatase inhibitor cocktail (catalog#78443, Thermo Scientific). The lysates were collected to separate tubes and put on ice for 30 min. During this period, we pipetted the lysates every 5 min. The supernatant was kept after centrifugation at 13,000 rpm for 10 min. Equal amounts of protein were loaded for SDS-polyacrylamide gel electrophoresis and electro-blotted onto equilibrated nitrocellulose membrane. After blocking in Tris-buffered saline (TBS) containing 5% non-fat milk, the membranes were immunoblotted with specific primary antibody overnight at 4 °C. ATF4/CREB-2 (1:200, Santa Cruz, sc390063), non-phospho β-catenin (1:1000, Cell Signaling, 8814), GAPDH (1:200, Santa Cruz, sc47724), α-Tubulin (1:2000, Abcam, ab7291) and β-actin (1:5000, Sigma, A1978) were used in this study. After washed with TBS containing 0.1% Tween 20 (TBST) for three times, the membranes were further incubated in HRP-conjugated antibodies (1:8000) and visualized by the enhanced chemiluminescence assay (GE Healthcare, UK) following the manufacturer's instructions. Image J software was used to determine the densitometry of western blots.

2.17. Measurement of intracellular Mg^{2+}

MLO-Y4 and MC3T3-E1 cells were seeded on cover glasses at a density of $1x10^4$ cells/cm^2. Collagen type I (Thermo, A1048301) was used to coat the cover glasses for better attachment of MLO-Y4 cells. 24 h after seeding, cells were incubated with Mg-Fura-2-AM (2 μM, Invitrogen, M1292) and Pluronic F-127 (1 μM, Life Technologies, USA) in the Mg^{2+}-free Margo-Ringer solution containing 130 mM NaCl, 5 mM KCl, 2.5 mM $CaCl_2$, 20 mM HEPES and 10 mM glucose (pH 7.4), for 30 min before washed with the Mg^{2+}−free Margo's solution and stabilized at room temperature for another 10 min. Cells on cover glasses were mounted to a mini-chamber, which was then placed on a microscope equipped with a CCD camera (Nikon Eclipse Ti, Japan). Every 5s, 340 and 380 nm excitations were alternatively used to excite Mg-Fura-2-AM in cells and the emitted fluorescent lights were collected at 510 nm, and pictures were taken.

2.18. cAMP assay

Cells were grown at density of $1.6x10^4$ cells/cm^2. Prior to the experiments, cells were incubated with low serum medium for 30 min before treated with 10 mM $MgCl_2$ or 20 mM NMDG-Cl as control in serum-free medium containing 100 μM IBMX (Sigma, 410957) for 15 min. Medium was then removed and 0.1 M HCl was added to lyse the cells. The lysates were centrifuged at 1000 g for 10 min to remove the cell debris before used in the cAMP ELISA kit (Enzo, ADI901–066).

2.19. Adenovirus-based knockdown of Atf4 in vitro and in vivo

Adenovirus-packaged shRNA or null sequence (purchased from Vector BioLabs, 10^9 PFU for single injection into the unilateral femoral marrow cavity) transfected femora in wild-type mice. Knockdown efficiency was evaluated with western blotting. The mice were pre-transfected with the Ad-GFP-U6-m*Atf4*-shRNA for 5 days in *Atf4*-KD group in the subsequent experiments. For *in vitro* experiment, the MC3T3-E1 cells were pre-transfected with the Ad-GFP-U6-m*Atf4*-shRNA (500 pfu/cell) for 72 h in *Atf4*-KD group.

2.20. Blockage of Wnt pathway in vivo using iCRT14

Following a previous study [25] and to continuously inhibit the Wnt pathway, mice were i.p. administered iCRT14 (50 mg/kg, every other day) until the end-point (12 weeks). No signs of systemic toxicity or weight loss was observed.

2.21. Measurement of serum Mg^{2+}

Inductively coupled plasma mass spectrometer (ICP-MS, Agilent Technologies, Tokyo, Japan) was used to quantitatively measure the Mg ion concentrations in serum, according to our previous study [26].

2.22. Statistical analyses

In this study, we randomly assigned sex- and age-matched animals into each group. We did not exclude any samples, animals, and data points. We conducted the analyses in a nonblinded fashion. We estimated sample size using both preliminary data and the observed effect sizes. We presented the quantitative data as means ± s.e.m., where n was defined as the number of tissue preparations, cells or animals. For comparison between two groups, we applied two-tailed Student's t-test. For multiple-group comparisons, we used one-way or two-way ANOVA with relevant *post hoc* tests which was indicated in separate figure legends. Regardless of statistical distribution, we used box-and-whisker plots to describe the entire population. We used GraphPad Prism software (Version 8) to perform statistical analysis and defined $P < 0.05$ as statistically significant.

3. Results

3.1. Magnesium implantation promotes bone formation in CFTR-deficient mice

To explore potential therapeutic effect of magnesium on CFBD, a mouse model carrying ΔF508, the most frequent mutation of CFTR causing its deficiency in CF, was used in the present study [20,27]. Pure magnesium or stainless-steel rods (as control) were surgically implanted (see Methods) into the medullary cavity of intact femora in wild-type or ΔF508 mice. At week 2, in both wild-type and ΔF508 mice, new bones were observed under micro-CT to be formed in the femora implanted with the magnesium rod (Fig. 1A&B). Longitudinal view of long bones showed that the cortical bones were thickened by magnesium implantation. Further quantitative analysis showed that in mice treated with control implants, the bone volume of both cortical and trabecular regions of femora was significantly lower in ΔF508 mice as compared to that in the wild-type, suggesting bone defects in ΔF508 mice. Magnesium implantation for 2 weeks significantly increased the bone volume of trabecular and cortical bones in both wild-type and ΔF508 mice. Moreover, the cortical and trabecular bone volume of femora in ΔF508 mice were brought up by the magnesium implant to levels comparable to that in the wild-type (Fig. 1C). The serum levels of bone turnover markers, procollagen I N-terminal peptide (PINP, a bone formation marker) and C-terminal telopeptides of type I collagen (CTX, a bone resorption marker), were also measured. In mice treated with control implants, the PINP level was found to be significantly lower in ΔF508 mice than that in the wild-types (Fig. 1D), consistently suggesting defective bone formation with CFTR deficiency. Magnesium implantation for 2 weeks elevated the PINP levels significantly in both wild-type and ΔF508 mice (Fig. 1D), with the PINP level in ΔF508 rescued to a level comparable to the wild-types. The CTX level did not show apparent difference between wild-type and ΔF508 mice implanted with magnesium or not (Fig. 1D). Remodeling assessment by calcein/xylenol double-labelling showed that with the control implant, the bone formation was significantly impaired in ΔF508 mice, as compared to the wild-type mice (Fig. 1E). The magnesium implant, as compared to the control implant, significantly accelerated bone formation in ΔF508 mice, raising their trabecular mineral apposition rate (MAR) and bone formation rate (BFR/BS) to a level comparable to that of the wild-type mice (Fig. 1F). These results altogether suggest the beneficial effect of magnesium implantation in facilitating bone formation despite CFTR deficiency.

3.2. Magnesium implantation improves bone fracture healing in CFTR-deficient mice

Since CFBD is associated with a high risk of fracture and its healing is often challenging, we next tested the effect of the magnesium implant on bone fracture healing in ΔF508 mice. A closed fracture model was established in ΔF508 mice (see Methods). As a pure magnesium rod degrades quickly *in vivo* and thus cannot provide prolonged physical support for fracture healing, we previously developed a magnesium-containing intramedullary nail (Mg-IMN, see Methods) [9]. In the present study, the Mg-IMN was adopted to fix the fracture in ΔF508 mice. At the early time point of healing (week 3 post implantation), the non-magnesium control nail (IMN) implanted-mice showed a callus size (as measured by X-ray images) in the fracture sites in ΔF508 mice that was much smaller than that of the wild-type mice (Fig. 2A), suggesting impaired fracture healing in ΔF508 mice. In contrast, implantation of Mg-IMN significantly increased the callus size and serum bone formation markers (osteocalcin and alkaline phosphatase activity), as compared to IMN-implanted ones, in ΔF508 mice (Fig. 2A&B). Also, histological staining showed that Mg-IMN effectively rescued the impaired callus formation at the early stage (week 2) as well as callus remodeling at the late stage (week 8) in ΔF508 mice (Fig. 2C). Consistent with these findings, *von kossa* staining showed Mg-IMN improved mineralization at the fracture gap during healing (week 4, mid-stage), whereas at the same stage of healing, a visible fracture gap remained in ΔF508 mice implanted with IMN (Fig. 2D). At week 12 post-fracture/implantation, micro-CT results (Fig. 2E) confirmed that Mg-IMN, as compared to IMN, enhanced ossification, resulting in increased bone volume and density in ΔF508 mice. Importantly, biomechanical testing indicated improved bone strength by Mg-IMN implantation in ΔF508 mice after healing from fracture for 12 weeks (Fig. 2F).

3.3. Magnesium implantation restores Wnt/β-catenin signaling to promote bone formation in CFTR-deficient mice

Given the observed beneficial effect of the magnesium implant on bone healing in the ΔF508 mice, we went on to explore the mechanism

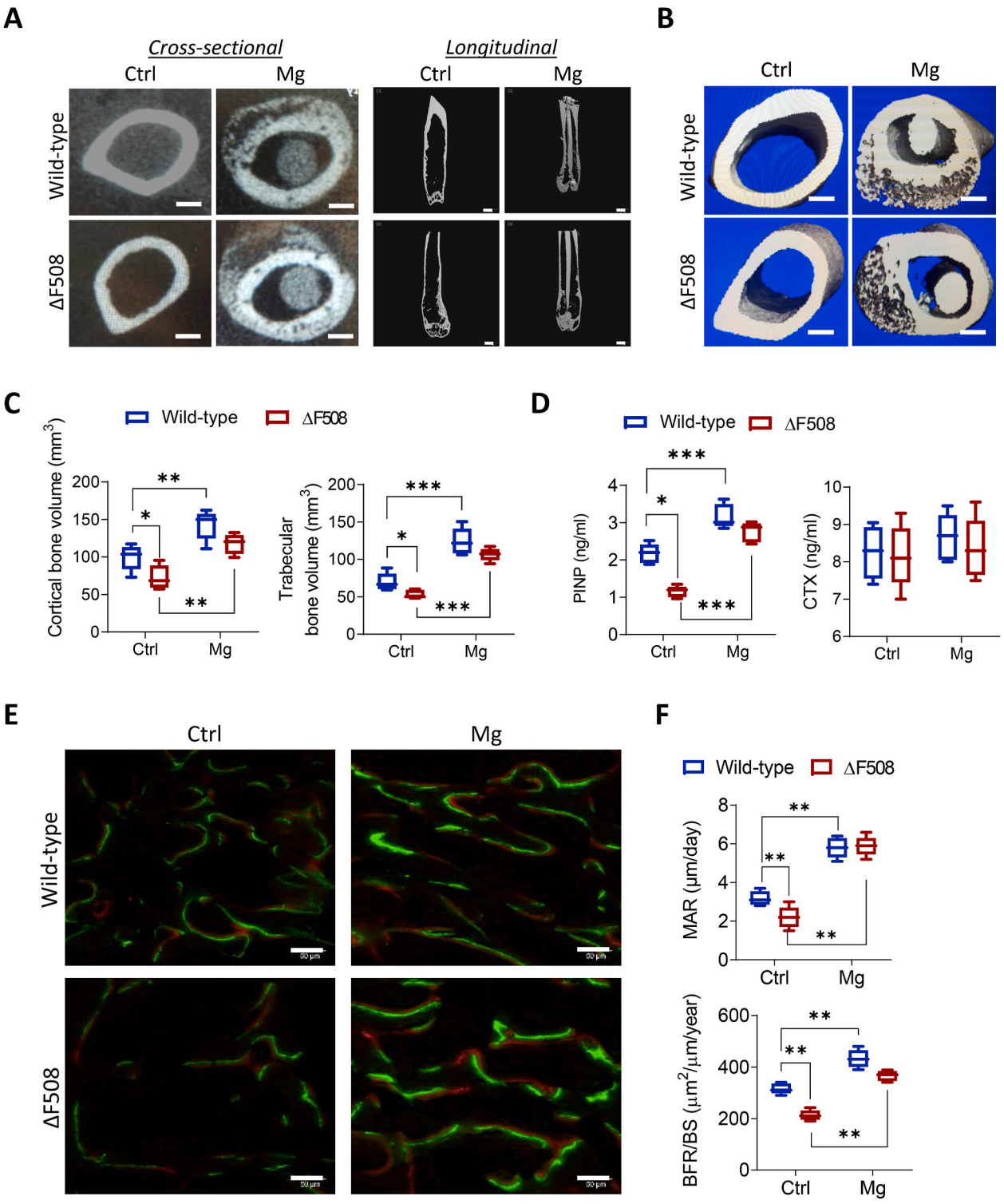

Fig. 1. Magnesium-implant induces bone formation in ΔF508 mice. (**A-C**) Representative cross-sectional images and longitudinal views from micro-CT scanning ($n = 5$ images from each group, A), 3D reconstructions (B), and corresponding quantitation of cortical and trabecular bone volumes (C) of femora (mid-shaft to distal) from ΔF508 or age-matched wild-type mice, implanted with magnesium rods (with a diameter of 0.5 mm) or stainless steel ones as the control (Ctrl) for 2 weeks. To avoid scanning artifact, stainless-steel implants were carefully removed from the bone before micro-CT. Scale bars, 500 μm $^{*}P < 0.05$, $^{**}P < 0.01$, $^{***}P < 0.001$ by one-way ANOVA with *Tukey's post hoc* test. $n = 5$ in each group. **(D)** ELISA measurement of serum levels of procollagen I N-terminal peptide (PINP, a bone formation marker) and C-terminal telopeptides of type I collagen (CTX, a bone resorption marker) in ΔF508 or age-matched wild-type mice implanted with magnesium rods (Mg) or stainless steel ones as the control (Ctrl) for 2 weeks. $^{*}P < 0.05$, $^{***}P < 0.001$ by one-way ANOVA with *Tukey's post hoc* test. $n = 5$ per group. (**E-F**) Bone-remodeling assessment by calcein/xylenol double-labeling with representative images in E and corresponding quantitation (F) of mineral apposition rate (MAR) and bone formation rate per bone surface (BFR/BS) in distal femora 2 weeks after implanted with Ctrl or magnesium rods. n = 5 mice for each group. Scale bars in panel F, 50 μm $^{**}P < 0.01$, from one-way ANOVA with *Tukey's post hoc* test. Data are means ± s.e.m.

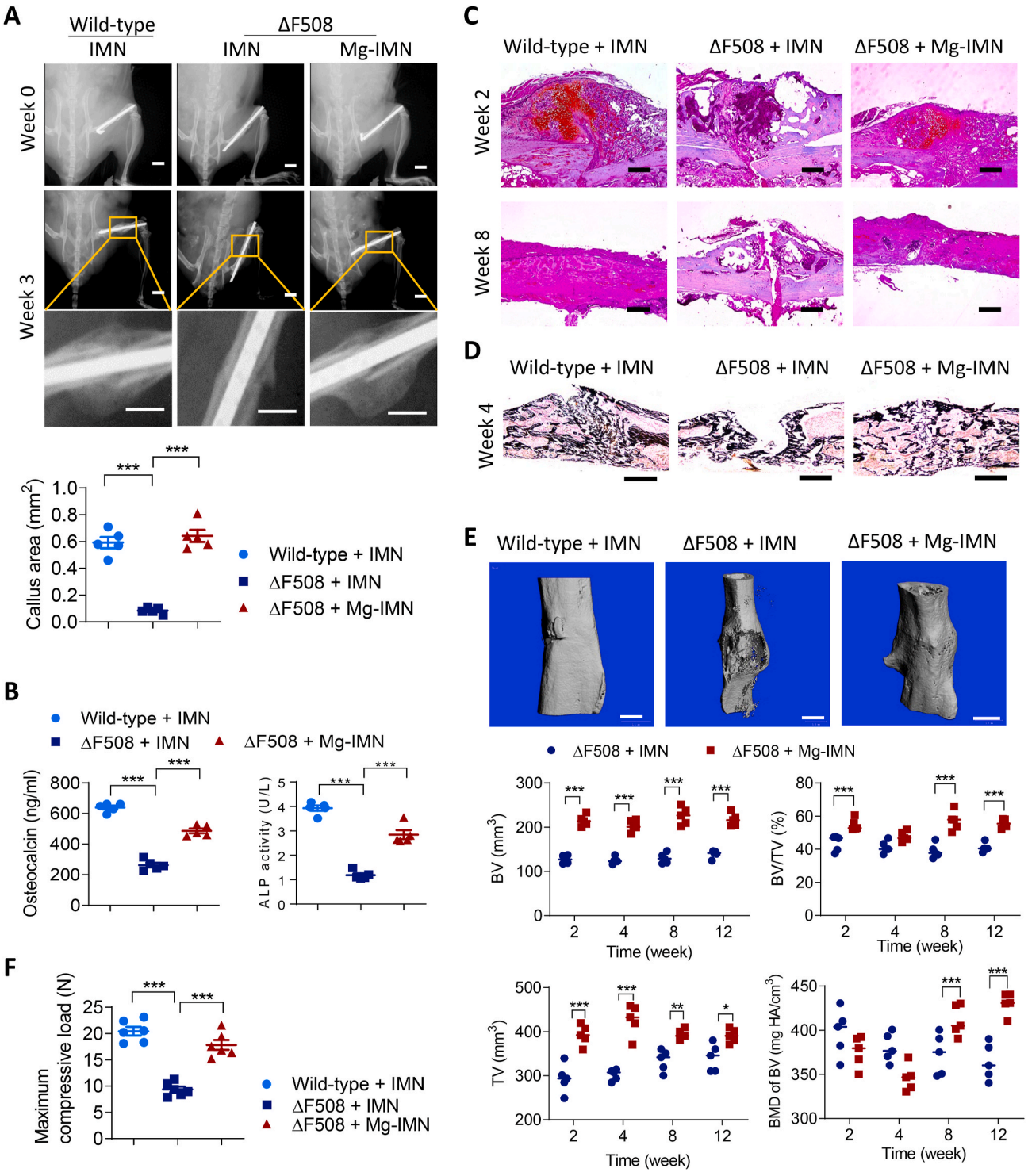

Fig. 2. Magnesium-inserted intramedullary nail (Mg-IMN) rescues the impaired fracture healing in ΔF508 mice. (**A**) Radiographs showing the femoral fracture healing (with fracture callus regions enlarged) 0 or 3 weeks after fractured and implanted with Mg-IMN or IMN (See methods) in wild-type or ΔF508 mice. The area of the callus at week 3 post-fracture was measured by Image J. Scale bars, 2 mm ***$P < 0.001$, from one-way ANOVA with *Tukey's post hoc* test. $n = 5$ in each group. (**B**) ELISA measurement of serum levels of alkaline phosphatase (ALP) and osteocalcin, two osteogenic markers, in indicated groups at week 3 post-fracture. ***$P < 0.001$, from one-way ANOVA with *Tukey's post hoc* test. $n = 5$ in each group. (**C**) Safranin O staining for assessment of endochondral ossification within the fracture callus ($n = 1$ image from each of five mice per group). Scale bars, 500 μm. (**D**) Assessment of bone mineralization via *von Kossa* staining. Calcium-rich region was stained in black. Scale bars, 1 mm. (**E**) Micro-CT 3D reconstructions and measurements of bone volume (BV), tissue volume (TV), and bone mineral density (BMD). Scale bars, 1 mm *$P < 0.05$, **$P < 0.01$, ***$P < 0.001$, from two-way ANOVA with *Tukey's post hoc* test. $n = 5$ in each group. The three-dimensional images show the healing status at week 12. (**F**) Three-point bending test for measuring the biomechanical strength of the healing bone at week 12. ***$P < 0.001$, from one-way ANOVA with *Tukey's post hoc* test. $n = 6$ in each group.

underlying magnesium's action. As we previously reported that magnesium can enhance CGRP production from sensory neurons to promote bone formation and fracture healing, the CGRP level in ΔF508 mice was examined. However, CGRP levels in the callus were found to be similar in ΔF508 and wild-type bones (Fig. S1). On the other hand, Wnt/β-catenin signaling was reported to be impaired in bone cells in ΔF508 mice [28]. We therefore tested if the impaired Wnt/β-catenin signaling with CFTR deficiency could be restored by magnesium. Indeed, the protein level of active β-catenin (non-phosphorylated), the key player in Wnt/β-catenin signaling, in the femora was found to be diminished in ΔF508 mice, as compared to the wild-type mice (Fig. 3A&B). At 2 weeks after a pure magnesium rod was inserted, the active β-catenin level was significantly raised in ΔF508 mice to a level that was comparable to the active β-catenin level in wild-type mice with magnesium (Fig. 3B). In the fracture model in ΔF508 mice, a PCR array was conducted to measure Wnt/β-catenin signaling target genes in the fracture callus with old cortical bone involving 2.5 mm below and above the fracture line (that is 5 mm in length) while excluding bone marrow in the medullary cavity. 78 genes out of 84 genes as assigned in the array plate were detectable in the samples (Fig. 3C). Many of these genes showed higher expression in femoral tissues treated with Mg-IMN, as compared to those with IMN. Among them, *Runx2*, a key transcription factor for bone formation, was found to be about 10-fold higher in Mg-IMN-treated femora versus IMN-treated ones (Fig. 3C).

To confirm the involvement of Wnt/β-catenin signaling in the action of magnesium on improving bone health, we next performed treatment of magnesium in conjunction with the inhibition of Wnt/β-catenin signaling by iCRT14, a β-catenin-responsive transcription inhibitor [25]. In the fracture model, after Mg-IMN implantation, iCRT14 (50 mg/kg body weight, every other day) was injected to surround the fracture site in each mouse for 12 weeks. MicroCT measurement of the bone fracture site showed that the enhancement of BV, TV, BV/TV and BMD by Mg-IMN over IMN, was significantly inhibited by the concurrent iCRT14 treatment (Fig. 3D), suggesting that the effect of magnesium is largely dependent on Wnt/β-catenin signaling.

3.4. Magnesium enters bone cells to activate ATF4 required for bone formation in CFTR-deficient mice

We next asked how magnesium can activate Wnt/β-catenin signaling to promote bone formation. Since both osteoblasts and osteocytes showed active β-catenin expression after treatment with magnesium (Fig. S2), two bone cell lines, an osteocyte-like, MLO-Y4, and a pre-osteoblast, MC3T3-E1, were used to test the direct effect of magnesium on bone cells. Using a Mg^{2+}-sensitive fluorescence dye, magnesium Fura-2 (Mg-Fura-2), to monitor intracellular Mg^{2+} level ($[Mg^{2+}]_i$), the addition of $MgCl_2$ (10 mM) into the extracellular bath induced an increase in $[Mg^{2+}]_i$ in MLO-Y4 cells, which was significantly higher compared to the response to NMDG-Cl (20 mM), a cell membrane-non-permeable cation as the control (Fig. 4A–C). Such an increase in $[Mg^{2+}]_i$ was attenuated by pretreating MLO-Y4 cells with blockers of magnesium channels/transporters: ruthenium red (50 μM, inhibitor for TRPM6 and TRPV), nitrendipine (50 μM, inhibitor for MAGT1), and 2-APB (100 μM, inhibitor for TRPM7), suggesting Mg^{2+} entry into the cells through these channels/transporter (Fig. 5B and C). Whereas, in MC3T3-E1 cells, no significant response to $MgCl_2$ was seen (Fig. 4D). Since Mg^{2+} is known to be crucial for adenylyl cyclase activity and cAMP production, the intracellular cAMP level in these two cell lines were also measured. The result showed that in MLO-Y4 cells treated with $MgCl_2$ (10 mM, 15 min) had an elevated intracellular cAMP level as compared to NMDG-Cl-treated cells (Fig. 4E). Whereas, in MC3T3 cells, the treatment with $MgCl_2$ did not alter intracellular cAMP level (Fig. 4E), consistent with the negligible Mg^{2+} entry (Fig. 4D) in this cell line. Given these observed differences between the two cell lines, the expression of reported Mg^{2+} transporters/channels in the two lines, which could possibly allow the entry of Mg^{2+}, were examined. Multiple Mg^{2+} transporters/channels were detected at mRNA level, and MLO-Y4 cells showed substantial higher (up to about 100 times for *Trpm6*) mRNA expression of Mg^{2+} channels/transporters including *Trpm6, Cldn16, Slc41a1, Slc41a2, Cnnm4* and *Nipa2* as compared to MC3T3 cells (Fig. 4F), which consistently suggested a higher capacity of MLO-Y4, the osteocyte-like line, in transporting and responding to Mg^{2+}.

Given its effect on intracellular cAMP in MLOY-4 cells, possible effect of Mg^{2+} on ATF4 (activating transcription factor 4), a cAMP-activated transcription factor known to regulate both bone formation and Wnt/β-catenin signalling [29–31], was examined. Immunofluorescence staining for ATF4 in MLO-Y4 cells (Fig. 4G) showed that ATF4 accumulated into the nucleus after cells were treated with $MgCl_2$ (10 mM) for 30 min. Whereas, in cells treated with NMDG-Cl (20 mM) as the control, ATF4 was found mostly in the cytoplasm (Fig. 4G). Also, total protein level of ATF4 was increased after treating MLO-Y4 cells with $MgCl_2$ (10 mM), as compared to that in cells treated with NMDG-Cl (20 mM) as the control (Fig. 4H). Consistent with these *in vitro* findings, both ATF4 and active β-catenin were upregulated in the osteocytes of neo-bone tissues within the fracture callus in the Mg-INM-treated group, as compared to IMN-treated group (Fig. 5A). To confirm the role of ATF4, *in vivo* ATF4 knockdown was adopted in conjunction with magnesium treatment in the fracture model. Virus containing ATF4-targeting shRNAs (10^9 pfu) were injected once at the femoral mid-shaft, which significantly blocked ATF4 expression by 80% in bone tissues in the mice for up to 3 weeks (Fig. 5B), suggesting a successful knockdown. With such ATF4 knockdown, active β-catenin induced by Mg-IMN was largely diminished (Fig. 5C). The enhanced BV, TV, BV/TV as well as mechanical strength of healed femora in ΔF508 mice by Mg-IMN were inhibited significantly with ATF4 knockdown (Fig. 5D and E), confirming that ATF4 is required for magnesium-induced Wnt/β-catenin activation and improved bone fracture healing with CFTR deficiency.

3.5. Oral supplementation with magnesium restores bone quality in CFTR-deficient bones

Given the promising effect of the magnesium implant, we went on to test if oral administration of magnesium can rescue bone fragility related to CFTR deficiency. Both wild-type and ΔF508 mice were treated with oral supplementation of magnesium (100 mg/kg/day). The treated mice were around 12-month-old and the serum Mg^{2+} level before treatment was similar between wild-type and ΔF508 mice (Fig. 6A). Two weeks after the oral treatment, the serum Mg^{2+} level was elevated by ~20% in both wild-type and ΔF508 mice, which was sustained until week 6 (Fig. 6A). We traced the bone mineral content (BMC) and BMD in ΔF508 mice for 6 weeks after the treatment and found that the whole-body BMC and BMD were significantly increased at week 4 and 6 as compared to baseline values at week 0 (Fig. 6B). Consistently, micro-CT analysis confirmed that BV, TV, BV/TV and BMD were significantly improved by oral magnesium in ΔF508 mice (Fig. 6C). Of note, in the wild-type mice, only a small effect of oral magnesium in increasing BMC (as measured by DXA), but not other parameters, was seen (Fig. 6B and C). Moreover, similar to the effect of magnesium implantation, 6 weeks' oral supplementation of magnesium in ΔF508 mice robustly increased serum level of PINP, a bone formation marker, but not CTX, a bone resorption marker (Fig. 6D). Western blotting was used to measure the expression of ATF4 and active β-catenin in the femoral bone lysates (Fig. 6E). Both ATF4 and active β-catenin were significantly elevated in femoral lysates from ΔF508 mice received oral supplementation of magnesium ions for 6 weeks as compared to age-matched ΔF508 without magnesium treatment, consistent with the effect of magnesium implantation. In wild-type mice, supplementation of magnesium ions at the same dose did not affect the expressions of both proteins (Fig. 6E).

4. Discussion

In summary, the present results have collectively shown that

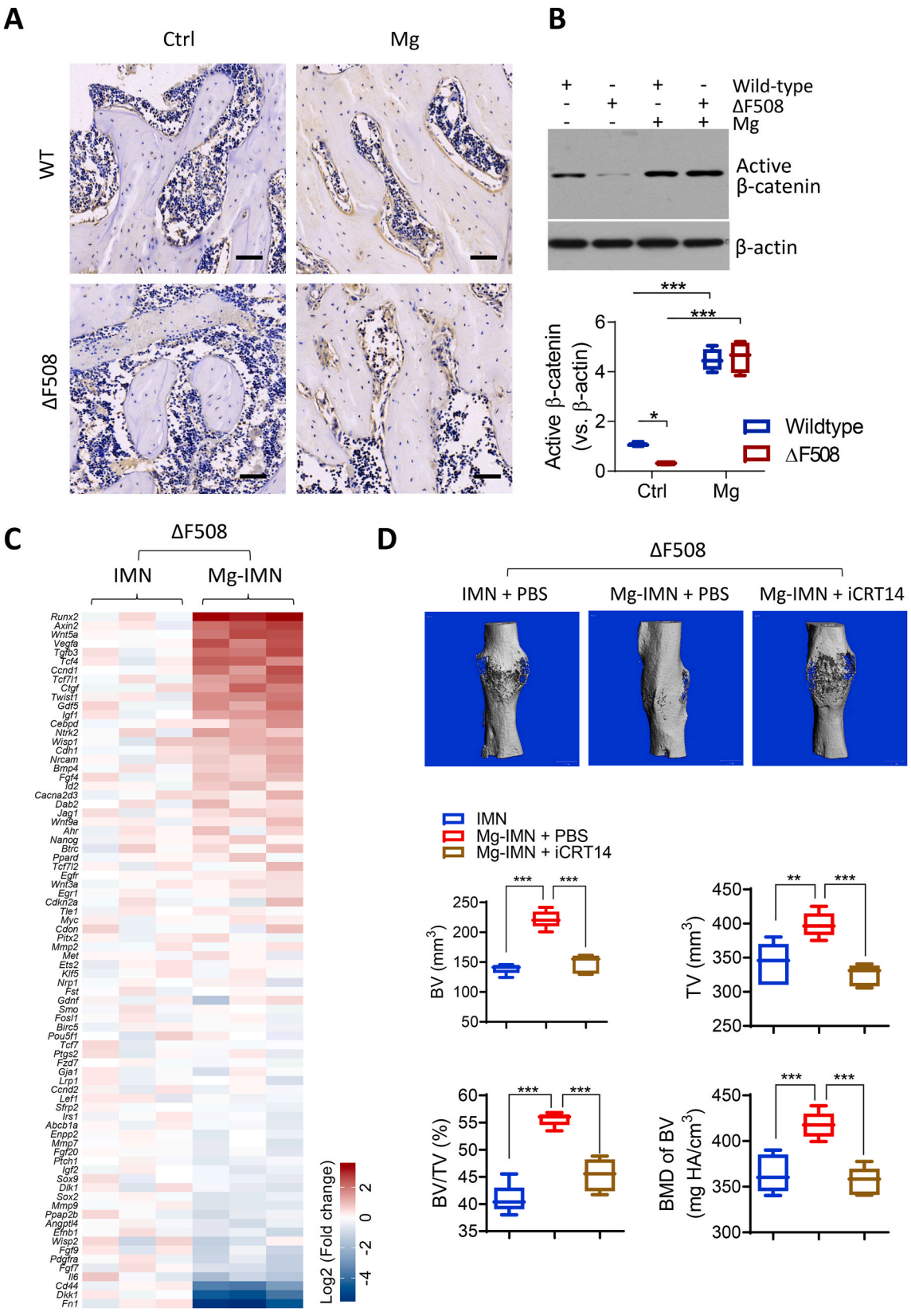

Fig. 3. Magnesium implantation restores Wnt/β-catenin signaling to promote bone formation in ΔF508 mice. (**A-B**) Immunohistochemical staining (A) and western blots with quantification (B) for non-phospho (active) β-catenin (Ser33/37/Thr41) in trabecular bone regions of distal femora collected at week 2 post implantation of Mg or IMN (Ctrl). Scale bars, 40 μm $^{*}P < 0.05$, $^{***}P < 0.001$, from one-way ANOVA with *Tukey's post hoc* test. $n = 3$ per group. (**C**) Quantitative PCR array for Wnt signaling target genes in bone tissues from ΔF508 mice at 2 weeks after implanted with IMN or Mg-IMN. Three biological replicates were presented. (**D**) Micro-CT measurements of TV, BV, and BMD at the midshaft of femora from ΔF508 mice implanted for 12 weeks with IMN or Mg-IMN with co-treatment with iCRT14 (i.p. 50 mg/kg, every other day), an inhibitor of Wnt signaling (ref [25]), or PBS as control. Scale bars, 1 mm $^{**}P < 0.01$, $^{***}P < 0.001$, from one-way ANOVA with *Tukey's post hoc* test. $n = 5$ per group. The 3D images show the healing status at week 12.

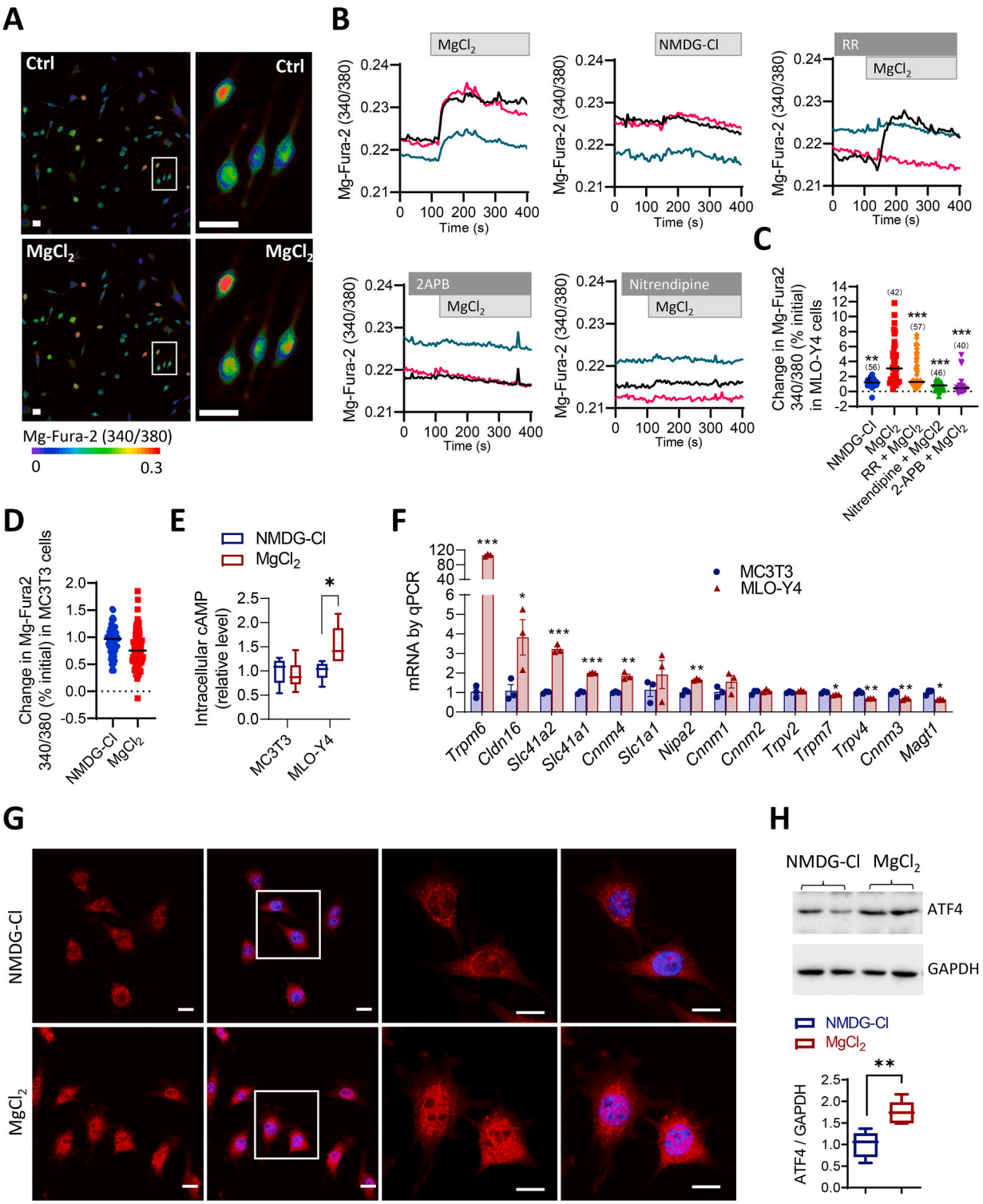

Fig. 4. Mg^{2+} enters bone cells to activate ATF4. (A–C) Representative images (A), time-course tracing (B) and corresponding quantification (C) of Mg-Fura-2 detection of intracellular Mg^{2+} level in MLO-Y4 cells in response to the addition of $MgCl_2$ (10 mM) or NMDG-Cl (20 mM, a non-cell membrane-permeable cation as the control) into Mg^{2+}-free bath with or without pretreatment with ruthenium red (RR, 50 μM, inhibitor for TRPM6 and TRPV), nitrendipine (50 μM, MAGT1 inhibitor) and 2-APB (100 μM, TRPM7 blocker). Scale bars, 50 μm. Pseudo colors purple/blue to yellow/red indicate fluorescence intensity from low to high. $^{***}P < 0.001$, from one-way ANOVA with *Tukey's post hoc* test. Sample size is shown in each column. **(D)** Intracellular Mg^{2+} levels in MC3T3-E1 cells treated with $MgCl_2$ or NMDG-Cl. **(E)** ELISA measurement of intracellular cAMP treated with $MgCl_2$ (10 mM) or NMDG-Cl (20 mM) as control for 15 min in MLO-Y4 and MC3T3 cells. **(F)** qPCR analysis of mRNA expression of Mg^{2+} channel/transporter genes in MC3T3 and MLO-Y4 cells. $^{*}P < 0.05$, $^{**}P < 0.01$, $^{***}P < 0.001$ by Student's t-test. **(G–H)** Immuno-fluorescent imaging (G) and western bloting of ATF4 in MLO-Y4 cells treated with $MgCl_2$ (10 mM) or NMDG-Cl (20 mM) as control for 30 min (G) or 48h (H). $^{**}P < 0.01$ by *t*-test. As loading control, GAPDH was used. Scale bars = 10 μm. DAPI was applied to stain the nuclei (in blue). (For interpretation of the references to color in this figure legend, the reader is referred to the Web version of this article.)

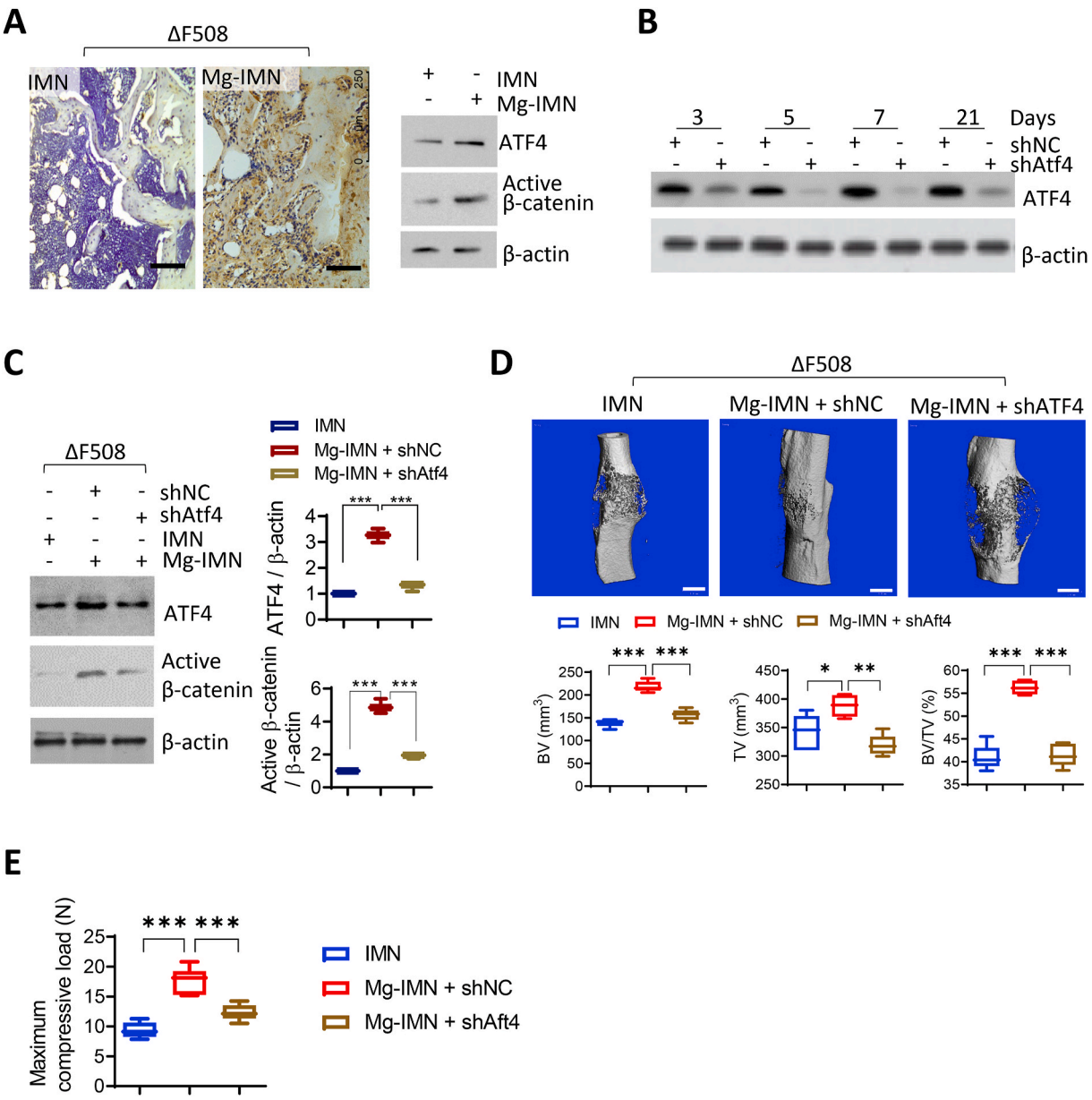

Fig. 5. ATF4 is required for magnesium-enhanced bone regeneration in ΔF508 mice. (A) Immunohistochemistry staining and western blotting for ATF4 in the fracture callus formed at the femoral mid-shafts at week 4 post fracture/implantation. Representative images were selected from three independent experiments. Scale bars, 100 μm. (**B**) Western blotting for ATF4 in mouse femora 3–21 days after treated with adenovirus-packaged shRNA against ATF4 (shAtf4, 10^9 PFU, single injection into the unilateral femoral marrow cavity), or non-silencing controls (shNC). (**C**) Western blotting for active β-catenin in femora of ΔF508 mice at 2 weeks after fractured and implanted with IMN or Mg-IMN. The mice were pre-transfected with shAtf4 or shNC 5 days before fracture/implantation. ***$P < 0.001$ by one-way ANOVA with *Tukey's post hoc* test. $n = 3$ in each group. (**D**) Representative Micro-CT 3D images with measurements of BV, TV, and BMD of femora in ΔF508 mice at 12 weeks after treated with IMN, Mg-IMN, shNC or shAtf4. Scale bars = 1 mm *$P < 0.05$, **$P < 0.01$, ***$P < 0.001$ by one-way ANOVA followed with *Tukey's post hoc* test. $n = 5$ in each group. (**E**) Three-point bending test for measuring the biomechanical strength of the healing bone at week 12. ***$P < 0.001$ by one-way ANOVA followed with *Tukey's post hoc* test. $n = 6$ in each group.

magnesium, by activating ATF4 and reversing the CFTR deficiency-impaired Wnt/β-catenin signaling, enhances bone formation, resulting in increased bone volume, density and strength as well as improved femoral fracture healing in bone diseases associated with CFTR deficiency (Fig. 7). It therefore highlights magnesium as a cost-effective approach with translational potential. The present study also shows successful application of magnesium-containing hybrid fixation systems in load-bearing bones, as summarized in our relatively recent reviews [8,32].

Consistent with previous observations in clinics as well as in animal models [16,33], the present study indicates a correlation of CFTR deficiency with bone defects. Several lines of evidence further suggest a bone formation problem with CFTR deficiency including 1) decreased serum level of bone formation markers (i.e. PINP, Osteocalcin, and ALP), 2) reduced MAR and BFR/BS, 3) downregulated Wnt/β-catenin signaling and 4) retarded fracture healing. In addition, bone resorption may not be active in ΔF508 mice, as suggested by the CTX serum level. Thus, impaired bone formation instead of enhanced bone resorption may underlie the osteoporotic phenotype in ΔF508 mice. In line with this observation, it should be noted that anti-resorptive drugs are of limited effect for CFBD [21,34]. Therefore, medications to favour bone formation (anabolic therapies) are needed for CFBD.

Magnesium, as the present study suggests, promotes bone formation or anabolic pathways. This is observed using either magnesium-

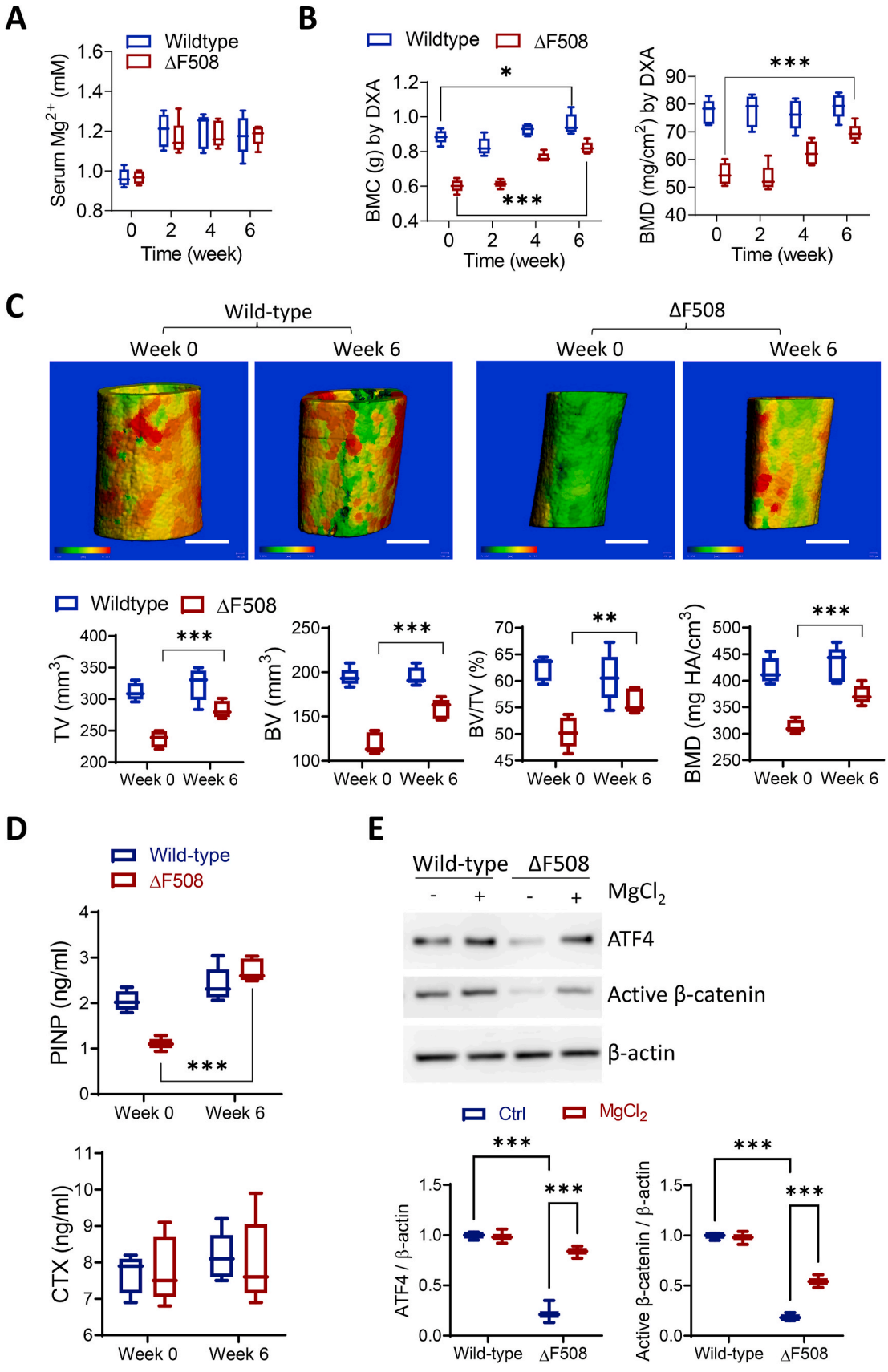

(caption on next page)

Fig. 6. Oral magnesium improves bone quality in ΔF508 bones. (A) Measurement of serum magnesium levels in wild-type and ΔF508 mice (n = 5) 0–6 weeks after oral administration of $MgCl_2$ (100 mg/kg body weight, per day). n = 5 per group. All the mice were 12-month-old when received the first oral administration. **(B)** DXA measurement of whole-body bone mineral content (BMC) and BMD in wild-type and ΔF508 mice 0–6 weeks after oral administration of $MgCl_2$ (100 mg/kg body weight, per day). $n = 5$ per group. $^{***}P < 0.001$ by two-way ANOVA with *Sidak's post hoc* test. **(C-D)** Micro-CT analysis of femoral mid-shaft (C) and ELISA measurement of serum levels of procollagen I N-terminal peptide (PINP) and C-terminal telopeptides of type I collagen (CTX, D) in wild-type and ΔF508 mice before (Week 0) and after (Week 6) oral administration of $MgCl_2$. White scale bars = 500 μm $^{**}P < 0.01$, $^{***}P < 0.001$ by Student's t-test. Pseudo-colors from green to yellow to red indicate bone thickness from thin to thick. All the mice were 12-month-old when they received the first oral administration (once per day). **(E)** Western blotting for ATF4 and active β-catenin in the protein lysates collected from the femoral mid-shafts excluding bone marrow at week 6 post magnesium supplementation. Age-matched mice of both genetic backgrounds without treatment were used as controls. Representative images were selected from three independent experiments. $^{***}P < 0.001$ by one-way ANOVA with *Tukey's post hoc* test. n = 3 in each group. (For interpretation of the references to color in this figure legend, the reader is referred to the Web version of this article.)

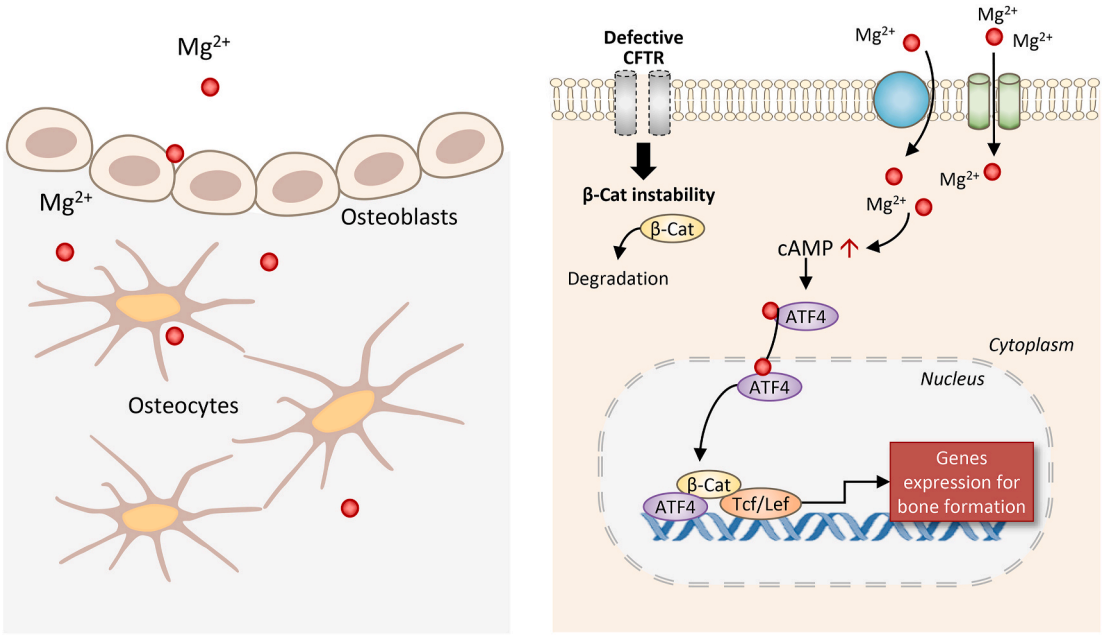

Fig. 7. Schematic diagram showing the effect of magnesium on bone formation with CFTR deficiency. Entering bone forming cells through Mg^{2+} channels or transporters, Mg^{2+} induces cAMP increase and the activation of transcription factors, ATF4 and β-catenin (β-Cat), rescuing CFTR-deficiency-impaired Wnt/β-catenin signaling to promote bone formation.

containing implants or magnesium oral supplementation, in both enhancing intact bones and improving bone fracture healing in ΔF508 mice. Moreover, the effect of magnesium may not be through inhibiting catabolic pathways, since the bone resorption marker is not altered by magnesium implant or oral supplementation. The present study for the first time, to the best of our knowledge, demonstrates that the osteogenic effect of magnesium could be directly on bone cells, in particular osteocytes. Mg^{2+} entry through Mg^{2+} transport/channels (e.g. TRPM6, TRPM7 and MAGT1) into bone cells were observed *in vitro*, which subsequently elevates intracellular cAMP level. Such an effect is most likely to be more active in osteocytes, given the observations that osteocyte-like MLO-Y4 cells have 1) higher expression of Mg^{2+} transport/channels, 2) larger Mg^{2+} entry and 3) more sensitive cAMP response to Mg^{2+} than that in the pre-osteoblast MC3T3-E1 cells. It should be noted that MLO-Y4 line is believed to be an early differentiation stage osteocyte line [35]. Osteocytes are the most abundant cell type in bone tissues actively involved in bone modeling and remodeling [35]. In recent years, studies have spotlighted the multifunctional roles of osteocytes in bone health and fracture healing [36–38]. Choy et al. highlighted the osteocyte-regulated events at gene, protein, cellular and tissue levels throughout the fracture healing phases in a systematic review [39]. Under osteoporotic fracture, osteocyte is also a determinant mediating the promotive effects of physical therapies including vibration and ultrasound [37,40]. The demonstration of magnesium's action on osteocytes provides a new mechanism underlying its beneficial function in promoting bone health.

Wnt/β-catenin signaling is critically involved in bone homeostasis including osteocyte functions [41]. Importantly, the present study has provided a set of evidence that an ATF4-dependent Wnt/β-catenin signaling may underlie magnesium's action, which includes ATF4 activation and upregulation by magnesium in osteocytes *in vitro* and bone tissues *in vivo*, as well as increase in active β-catenin level and activation of Wnt/β-catenin target genes by magnesium implant *in vivo*. It is further strongly supported by results that either blocking Wnt/β-catenin signaling or knockdown of ATF4 largely attenuated the effect of magnesium in ΔF508 mice, in line with a previous study reporting that ATF4 overexpression increased the expression of β-catenin and formed ATF4-β-catenin protein complex in osteoblast [31]. Therefore, the effect of magnesium on bones *in vivo* is probably manifold. On one hand, it enhances Wnt/β-catenin signaling in bone cells directly as we show here, while on the other hand, it can also promote neuronal production of CGRP as we previously reported [9]. It should be noted that not all examined Wnt/β-catenin target genes were promoted by magnesium. For example, *Dkk-1,* though a downstream of Wnt/β-catenin signaling [42], is significantly decreased by magnesium implantation. However, since *Dkk-1* is an inhibiting factor for bone formation, its down-regulation is consistent with the osteogenic effect of magnesium. It therefore suggests the involvement of additional regulatory mechanism underlying the action of magnesium, which awaits further investigation. Interestingly, it is believed that in the fracture models, the alkaline environment and hydrogen accumulation around the magnesium implant may also contribute to the promoted bone regeneration [43,44].

CFTR is closely related to extracellular pH regulation in other systems including the airway [1,45–47]. It is possible that magnesium may help correct pH disruption in CF too, which awaits further investigation. Systematic approaches such as transcriptomics or proteomics with further *in vitro* and *in vivo* investigations (e.g. osteocyte specific knockout models) will be needed to elucidate the underlying mechanisms in future.

It should be noted that the effect of oral magnesium supplementation has been tested in healthy, osteoporotic and post-menopausal osteoporotic subjects by other studies, which has yielded controversial results [48]. In the present study, in wild-type mice, only a small increase in BMC was seen by oral magnesium, while ΔF508 mice presented with significant increase in BMC and BMD after oral supplementation of magnesium. A possible reason for such variation is that genes and signaling pathways sensitive to magnesium may be substantially changed with CFTR deficiency, for example, ATF and Wnt/β-catenin signaling. The oral supplementation experiment in the present study may serve as a starting point and more in-depth investigations will be further implemented in the future. For instance, it is recommended to evaluate whether the effect of oral magnesium can be reversed by iCRT14 to consolidate the involvement of Wnt/β-catenin signaling. Since anabolic therapy for osteoporosis is still lacking [49], whether the presently demonstrated anabolic stimulating effect of magnesium can benefit other osteoporotic conditions (e.g. age-dependent, post-menopausal, disuse osteoporosis) may worth further investigation. Magnesium ion can synergize with either simvastatin or vitamin C to attenuate steroid-associated osteonecrosis [50], high-fat-diet induced bone loss [3], and osteoarthritis [2], suggesting its broad applications in skeletal diseases beyond CFBD.

The newly demonstrated role of magnesium in enhancing ATF4-dependent Wnt/β-catenin signaling may be far beyond benefiting CFBD, given the versatile roles of Wnt/β-catenin signaling in multiple physiological and pathophysiological events [41,51]. Magnesium deficiency or metabolism disturbance has been documented in subjects with CF with advanced age or who have severe pathology [22]. Intracellular Mg^{2+} is also critically involved in CFTR channel function [23]. The potential of magnesium in treating symptoms of other organs/systems in CF may warrant further exploration.

CRediT authorship contribution statement

Jiankun Xu: conception and design, experiments and data analysis, article writing with contributions from other authors. **Peijie Hu:** experiments and data analysis, article writing with contributions from other authors. **Xiaotian Zhang:** experiments and data analysis. **Junjiang Chen:** experiments and data analysis. **Jiali Wang:** experiments and data analysis. **Jieting Zhang:** experiments and data analysis. **Ziyi Chen:** experiments and data analysis. **Mei Kuen Yu:** experiments and data analysis. **Yiu Wa Chung:** experiments and data analysis. **Yan Wang:** experiments and data analysis. **Xiaohu Zhang:** experiments and data analysis. **Yifeng Zhang:** experiments and data analysis. **Nianye Zheng:** experiments and data analysis. **Hao Yao:** experiments and data analysis. **Jiang Yue:** experiments and data analysis. **Hsiao Chang Chan:** conception and design. **Ling Qin:** conception and design. **Ye Chun Ruan:** conception and design, article writing with contributions from other authors.

Declaration of competing interest

The authors declare no competing interests.

Acknowledgement

The work was supported in part by Theme-based Research Scheme of Hong Kong (No. T13-402/17 N), Health and Medical Research Fund of Hong Kong (15161441 and 18190481), Early Career Scheme of Hong Kong (No. 24104517), Start-up fund at the Hong Kong Polytechnic University, National Natural Science Foundation of China (81802152) and Natural Science Foundation of Guangdong Province (2019A1515012224 and 2021A1515011204).

Appendix A. Supplementary data

Supplementary data to this article can be found online at https://doi.org/10.1016/j.bioactmat.2021.06.034.

References

[1] X.D. Chen, Magnesium-based implants: beyond fixators, J. Orthopaedic Transl. 10 (2017) 1–4.
[2] H. Yao, J. Xu, J. Wang, Y. Zhang, N. Zheng, J. Yue, J. Mi, L. Zheng, B. Dai, W. Huang, S. Yung, P. Hu, Y. Ruan, Q. Xue, K. Ho, L. Qin, Combination of magnesium ions and vitamin C alleviates synovitis and osteophyte formation in osteoarthritis of mice, Bioact. Mater. 6 (5) (2021) 1341–1352.
[3] B. Dai, X. Li, J. Xu, Y. Zhu, L. Huang, W. Tong, H. Yao, D.H. Chow, L. Qin, Synergistic effects of magnesium ions and simvastatin on attenuation of high-fat diet-induced bone loss, Bioact. Mater. 6 (8) (2021) 2511–2522.
[4] M. Hamushan, W. Cai, Y. Zhang, Z. Ren, J. Du, S. Zhang, C. Zhao, P. Cheng, X. Zhang, H. Shen, P. Han, High-purity magnesium pin enhances bone consolidation in distraction osteogenesis via regulating Ptch protein activating Hedgehog-alternative Wnt signaling, Bioact. Mater. 6 (6) (2021) 1563–1574.
[5] D. Zhao, S. Huang, F. Lu, B. Wang, L. Yang, L. Qin, K. Yang, Y. Li, W. Li, W. Wang, S. Tian, X. Zhang, W. Gao, Z. Wang, Y. Zhang, X. Xie, J. Wang, J. Li, Vascularized bone grafting fixed by biodegradable magnesium screw for treating osteonecrosis of the femoral head, Biomaterials 81 (2015) 84–92.
[6] L. Chen, Z. Lin, M. Wang, W. Huang, J. Ke, D. Zhao, Q. Yin, Y. Zhang, Treatment of trauma-induced femoral head necrosis with biodegradable pure Mg screw-fixed pedicle iliac bone flap, J. Orthopaedic Transl. 17 (2019) 133–137.
[7] J.W. Lee, H.S. Han, K.J. Han, J. Park, H. Jeon, M.R. Ok, H.K. Seok, J.P. Ahn, K. E. Lee, D.H. Lee, S.J. Yang, S.Y. Cho, P.R. Cha, H. Kwon, T.H. Nam, J.H. Han, H. J. Rho, K.S. Lee, Y.C. Kim, D. Mantovani, Long-term clinical study and multiscale analysis of in vivo biodegradation mechanism of Mg alloy, Proc. Natl. Acad. Sci. U. S. A. 113 (3) (2016) 716–721.
[8] L. Tian, N. Tang, T. Ngai, C. Wu, Y. Ruan, L. Huang, L. Qin, Hybrid fracture fixation systems developed for orthopaedic applications: a general review, J. Orthop. Translat. 16 (2019) 1–13.
[9] Y. Zhang, J. Xu, Y.C. Ruan, M.K. Yu, M. O'Laughlin, H. Wise, D. Chen, L. Tian, D. Shi, J. Wang, S. Chen, J.Q. Feng, D.H. Chow, X. Xie, L. Zheng, L. Huang, S. Huang, K. Leung, N. Lu, L. Zhao, H. Li, D. Zhao, X. Guo, K. Chan, F. Witte, H. C. Chan, Y. Zheng, L. Qin, Implant-derived magnesium induces local neuronal production of CGRP to improve bone-fracture healing in rats, Nat. Med. 22 (10) (2016) 1160–1169.
[10] M.J. Welsh, A.E. Smith, Molecular mechanisms of CFTR chloride channel dysfunction in cystic fibrosis, Cell 73 (7) (1993) 1251–1254.
[11] F.S. Collins, Cystic fibrosis: molecular biology and therapeutic implications, Science 256 (5058) (1992) 774–779.
[12] J.H. Guo, H. Chen, Y.C. Ruan, X.L. Zhang, X.H. Zhang, K.L. Fok, L.L. Tsang, M. K. Yu, W.Q. Huang, X. Sun, Y.W. Chung, X. Jiang, Y. Sohma, H.C. Chan, Glucose-induced electrical activities and insulin secretion in pancreatic islet beta-cells are modulated by CFTR, Nat. Commun. 5 (2014) 4420.
[13] H.C. Chan, Y.C. Ruan, Q. He, M.H. Chen, H. Chen, W.M. Xu, W.Y. Chen, C. Xie, X. H. Zhang, Z. Zhou, The cystic fibrosis transmembrane conductance regulator in reproductive health and disease, J. Physiol. 587 (Pt 10) (2009) 2187–2195.
[14] D.A. Stoltz, D.K. Meyerholz, M.J. Welsh, Origins of cystic fibrosis lung disease, N. Engl. J. Med. 372 (4) (2015) 351–362.
[15] M. Marquette, C.S. Haworth, Bone health and disease in cystic fibrosis, Paediatr. Respir. Rev. 20 (Suppl) (2016) 2–5.
[16] R.M. Aris, P.A. Merkel, L.K. Bachrach, D.S. Borowitz, M.P. Boyle, S.L. Elkin, T. A. Guise, D.S. Hardin, C.S. Haworth, M.F. Holick, P.M. Joseph, K. O'Brien, E. Tullis, N.B. Watts, T.B. White, Guide to bone health and disease in cystic fibrosis, J. Clin. Endocrinol. Metab. 90 (3) (2005) 1888–1896.
[17] J. Paccou, N. Zeboulon, C. Combescure, L. Gossec, B. Cortet, The prevalence of osteoporosis, osteopenia, and fractures among adults with cystic fibrosis: a systematic literature review with meta-analysis, Calcif. Tissue Int. 86 (1) (2010) 1–7.
[18] S.L. Elkin, A. Fairney, S. Burnett, M. Kemp, P. Kyd, J. Burgess, J.E. Compston, M. E. Hodson, Vertebral deformities and low bone mineral density in adults with cystic fibrosis: a cross-sectional study, Osteoporos. Int. 12 (5) (2001) 366–372.
[19] Vertex CF triple drug roars to approval, Nat. Biotechnol. 37 (12) (2019) 1386.
[20] C.K. Haston, W. Li, A. Li, M. Lafleur, J.E. Henderson, Persistent osteopenia in adult cystic fibrosis transmembrane conductance regulator-deficient mice, Am. J. Respir. Crit. Care Med. 177 (3) (2008) 309–315.
[21] I. Sermet-Gaudelus, M.L. Bianchi, M. Garabedian, R.M. Aris, A. Morton, D. S. Hardin, S.L. Elkin, J.E. Compston, S.P. Conway, M. Castanet, S. Wolfe, C. S. Haworth, European cystic fibrosis bone mineralisation guidelines, J. Cyst. Fibros. 10 (Suppl 2) (2011) S16–S23.

[22] M. Santi, G.P. Milani, G.D. Simonetti, E.F. Fossali, M.G. Bianchetti, S.A. Lava, Magnesium in cystic fibrosis–Systematic review of the literature, Pediatr. Pulmonol. 51 (2) (2016) 196–202.
[23] M.F. Tsai, H. Shimizu, Y. Sohma, M. Li, T.C. Hwang, State-dependent modulation of CFTR gating by pyrophosphate, J. Gen. Physiol. 133 (4) (2009) 405–419.
[24] D.H. Chow, L. Zheng, L. Tian, K.S. Ho, L. Qin, X. Guo, Application of ultrasound accelerates the decalcification process of bone matrix without affecting histological and immunohistochemical analysis, J. Orthop. Translat. 17 (2019) 112–120.
[25] F.C. Gonsalves, K. Klein, B.B. Carson, S. Katz, L.A. Ekas, S. Evans, R. Nagourney, T. Cardozo, A.M. Brown, R. DasGupta, An RNAi-based chemical genetic screen identifies three small-molecule inhibitors of the Wnt/wingless signaling pathway, Proc. Natl. Acad. Sci. U. S. A. 108 (15) (2011) 5954–5963.
[26] J. Wang, F. Witte, T. Xi, Y. Zheng, K. Yang, Y. Yang, D. Zhao, J. Meng, Y. Li, W. Li, K. Chan, L. Qin, Recommendation for modifying current cytotoxicity testing standards for biodegradable magnesium-based materials, Acta Biomater. 21 (2015) 237–249.
[27] C. Le Henaff, A. Gimenez, E. Hay, C. Marty, P. Marie, J. Jacquot, The F508del mutation in cystic fibrosis transmembrane conductance regulator gene impacts bone formation, Am. J. Pathol. 180 (5) (2012) 2068–2075.
[28] C. Le Henaff, R. Mansouri, D. Modrowski, M. Zarka, V. Geoffroy, C. Marty, N. Tarantino, E. Laplantine, P.J. Marie, Increased NF-kappaB activity and decreased wnt/beta-catenin signaling mediate reduced osteoblast differentiation and function in DeltaF508 cystic fibrosis transmembrane conductance regulator (CFTR) mice, J. Biol. Chem. 290 (29) (2015) 18009–18017.
[29] X. Yang, G. Karsenty, ATF4, the osteoblast accumulation of which is determined post-translationally, can induce osteoblast-specific gene expression in non-osteoblastic cells, J. Biol. Chem. 279 (45) (2004) 47109–47114.
[30] X. Yang, K. Matsuda, P. Bialek, S. Jacquot, H.C. Masuoka, T. Schinke, L. Li, S. Brancorsini, P. Sassone-Corsi, T.M. Townes, A. Hanauer, G. Karsenty, ATF4 is a substrate of RSK2 and an essential regulator of osteoblast biology; implication for Coffin-Lowry Syndrome, Cell 117 (3) (2004) 387–398.
[31] S. Yu, K. Zhu, Y. Lai, Z. Zhao, J. Fan, H.J. Im, D. Chen, G. Xiao, atf4 promotes beta-catenin expression and osteoblastic differentiation of bone marrow mesenchymal stem cells, Int. J. Biol. Sci. 9 (3) (2013) 256–266.
[32] J.L. Wang, J.K. Xu, C. Hopkins, D.H. Chow, L. Qin, Biodegradable magnesium-based implants in orthopedics-A general review and perspectives, Adv. Sci. 7 (8) (2020) 1902443.
[33] J. Jacquot, M. Delion, S. Gangloff, J. Braux, F. Velard, Bone disease in cystic fibrosis: new pathogenic insights opening novel therapies, Osteoporos. Int. 27 (4) (2016) 1401–1412.
[34] J.S. Chen, P.N. Sambrook, Antiresorptive therapies for osteoporosis: a clinical overview, Nat. Rev. Endocrinol. 8 (2) (2011) 81–91.
[35] S.L. Dallas, M. Prideaux, L.F. Bonewald, The osteocyte: an endocrine cell and more, Endocr. Rev. 34 (5) (2013) 658–690.
[36] W.H. Cheung, R.M.Y. Wong, V.M.H. Choy, M.C.M. Li, K.Y.K. Cheng, S.K.H. Chow, Enhancement of osteoporotic fracture healing by vibration treatment: the role of osteocytes, Injury 52 (Suppl 2) (2021) S97–S100.
[37] T. Shimizu, N. Fujita, K. Tsuji-Tamura, Y. Kitagawa, T. Fujisawa, M. Tamura, M. Sato, Osteocytes as main responders to low-intensity pulsed ultrasound treatment during fracture healing, Sci. Rep. 11 (1) (2021) 10298.
[38] F.G.F. Tresguerres, J. Torres, J. Lopez-Quiles, G. Hernandez, J.A. Vega, I. F. Tresguerres, The osteocyte: a multifunctional cell within the bone, Ann. Anat. 227 (2020) 151422.
[39] M.H.V. Choy, R.M.Y. Wong, S.K.H. Chow, M.C. Li, Y.N. Chim, T.K. Li, W.T. Ho, J.C. Y. Cheng, W.H. Cheung, How much do we know about the role of osteocytes in different phases of fracture healing? A systematic review, J. Orthop. Translat. 21 (2020) 111–121.
[40] M.V. Choy, R.M. Wong, M.C. Li, B.Y. Wang, X.D. Liu, W. Lee, J.C. Cheng, S. K. Chow, W.H. Cheung, Can we enhance osteoporotic metaphyseal fracture healing through enhancing ultrastructural and functional changes of osteocytes in cortical bone with low-magnitude high-frequency vibration? Faseb. J. 34 (3) (2020) 4234–4252.
[41] R. Baron, M. Kneissel, WNT signaling in bone homeostasis and disease: from human mutations to treatments, Nat. Med. 19 (2) (2013) 179–192.
[42] A. Niida, T. Hiroko, M. Kasai, Y. Furukawa, Y. Nakamura, Y. Suzuki, S. Sugano, T. Akiyama, DKK1, a negative regulator of Wnt signaling, is a target of the beta-catenin/TCF pathway, Oncogene 23 (52) (2004) 8520–8526.
[43] S. Castiglioni, A. Cazzaniga, W. Albisetti, J.A. Maier, Magnesium and osteoporosis: current state of knowledge and future research directions, Nutrients 5 (8) (2013) 3022–3033.
[44] J. Eisinger, D. Clairet, Effects of silicon, fluoride, etidronate and magnesium on bone mineral density: a retrospective study, Magnes. Res. 6 (3) (1993) 247–249.
[45] J.D. Guo, L. Li, Y.M. Shi, H.D. Wang, S.X. Hou, Hydrogen water consumption prevents osteopenia in ovariectomized rats, Br. J. Pharmacol. 168 (6) (2013) 1412–1420.
[46] Y. Sun, F. Shuang, D.M. Chen, R.B. Zhou, Treatment of hydrogen molecule abates oxidative stress and alleviates bone loss induced by modeled microgravity in rats, Osteoporos. Int. 24 (3) (2013) 969–978.
[47] J. Tang, J. Wang, X. Xie, P. Zhang, Y. Lai, Y. Li, L. Qin, Surface coating reduces degradation rate of magnesium alloy developed for orthopaedic applications, J. Orthopaedic Transl. 1 (1) (2013) 41–48.
[48] V.S. Shah, D.K. Meyerholz, X.X. Tang, L. Reznikov, M. Abou Alaiwa, S.E. Ernst, P. H. Karp, C.L. Wohlford-Lenane, K.P. Heilmann, M.R. Leidinger, P.D. Allen, J. Zabner, P.B. McCray Jr., L.S. Ostedgaard, D.A. Stoltz, C.O. Randak, M.J. Welsh, Airway acidification initiates host defense abnormalities in cystic fibrosis mice, Science 351 (6272) (2016) 503–507.
[49] E.G. Estell, C.J. Rosen, Emerging insights into the comparative effectiveness of anabolic therapies for osteoporosis, Nat. Rev. Endocrinol. 17 (1) (2021) 31–46.
[50] L.Z. Zheng, J.L. Wang, J.K. Xu, X.T. Zhang, B.Y. Liu, L. Huang, R. Zhang, H.Y. Zu, X. He, J. Mi, Q.Q. Pang, X.L. Wang, Y.C. Ruan, D.W. Zhao, L. Qin, Magnesium and vitamin C supplementation attenuates steroid-associated osteonecrosis in a rat model, Biomaterials 238 (2020) 119828.
[51] B.T. MacDonald, K. Tamai, X. He, Wnt/beta-catenin signaling: components, mechanisms, and diseases, Dev. Cell 17 (1) (2009) 9–26.